JACS
JOURNAL OF THE AMERICAN CHEMICAL SOCIETY
Article
pubs.acs.org/JACS

Importance of the Donor:Fullerene Intermolecular Arrangement for High-Efficiency Organic Photovoltaics

Kenneth R. Graham,[†,‡] Clement Cabanetos,[‡] Justin P. Jahnke,[§] Matthew N. Idso,[§] Abdulrahman El Labban,[‡] Guy O. Ngongang Ndjawa,[‡] Thomas Heumueller,[†] Koen Vandewal,[†] Alberto Salleo,[†] Bradley F. Chmelka,[§] Aram Amassian,*[,‡] Pierre M. Beaujuge,*[,‡] and Michael D. McGehee*[,†]

[†]Department of Materials Science and Engineering, Stanford University, Stanford, California 94305, United States
[‡]Division of Physical Sciences & Engineering, King Abdullah University of Science and Technology (KAUST), Thuwal 23955-6900, Saudi Arabia
[§]Department of Chemical Engineering, University of California, Santa Barbara, California 93106, United States

Supporting Information

ABSTRACT: The performance of organic photovoltaic (OPV) material systems are hypothesized to depend strongly on the intermolecular arrangements at the donor:fullerene interfaces. A review of some of the most efficient polymers utilized in polymer:fullerene PV devices, combined with an analysis of reported polymer donor materials wherein the same conjugated backbone was used with varying alkyl substituents, supports this hypothesis. Specifically, the literature shows that higher-performing donor−acceptor type polymers generally have acceptor moieties that are sterically accessible for interactions with the fullerene derivative, whereas the corresponding donor moieties tend to have branched alkyl substituents that sterically hinder interactions with the fullerene. To further explore the idea that the most beneficial polymer:fullerene arrangement involves the fullerene docking with the acceptor moiety, a family of benzo[1,2-b:4,5-b′]dithiophene−thieno[3,4-*c*]pyrrole-4,6-dione polymers (PBDTTPD derivatives) was synthesized and tested in a variety of PV device types with vastly different aggregation states of the polymer. In agreement with our hypothesis, the PBDTTPD derivative with a more sterically accessible acceptor moiety and a more sterically hindered donor moiety shows the highest performance in bulk-heterojunction, bilayer, and low-polymer concentration PV devices where fullerene derivatives serve as the electron-accepting materials. Furthermore, external quantum efficiency measurements of the charge-transfer state and solid-state two-dimensional (2D) $^{13}C\{^{1}H\}$ heteronuclear correlation (HETCOR) NMR analyses support that a specific polymer:fullerene arrangement is present for the highest performing PBDTTPD derivative, in which the fullerene is in closer proximity to the acceptor moiety of the polymer. This work demonstrates that the polymer:fullerene arrangement and resulting intermolecular interactions may be key factors in determining the performance of OPV material systems.

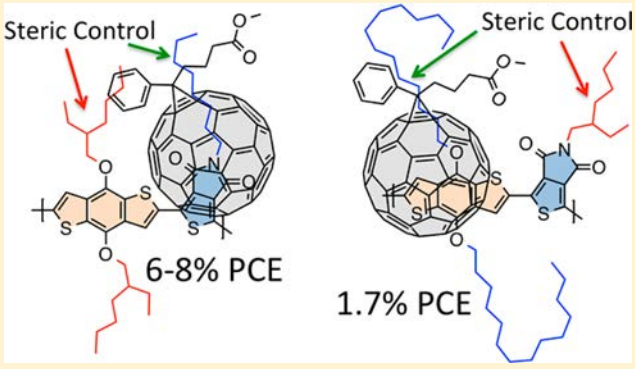

INTRODUCTION

Organic photovoltaics (OPVs) are a promising PV technology due to their use of potentially low-cost and nontoxic materials, high performance in low light conditions, and their potential for solution processing on inexpensive flexible substrates.[1−3] Critical to the operation of an organic photovoltaic (OPV) device is the interface between an electron-donating material and an electron-accepting material, where photogenerated excitons are dissociated and separated into free charges. It is expected that the molecular arrangement at this interface and the resulting interfacial energetics play a major role in exciton dissociation, charge separation, and charge recombination processes,[4] yet this important role remains to be clearly established.

Although hundreds, or even thousands, of OPV materials have been synthesized and studied,[1,5−9] many questions still remain as to what factors actually make a high-performing OPV material. Some material properties that can lead to high performance are known, such as reasonably high charge-carrier mobility, broad and strong absorbance, and appropriate energy levels to form a type II heterojunction. However, many systems that display these properties yield only moderate or low performance,[9−14] potentially because the intermolecular arrangements and resulting energy landscapes at the donor−acceptor interface are unfavorable for charge separation. The

Received: March 27, 2014
Published: June 16, 2014

dx.doi.org/10.1021/ja502985g | J. Am. Chem. Soc. 2014, 136, 9608−9618

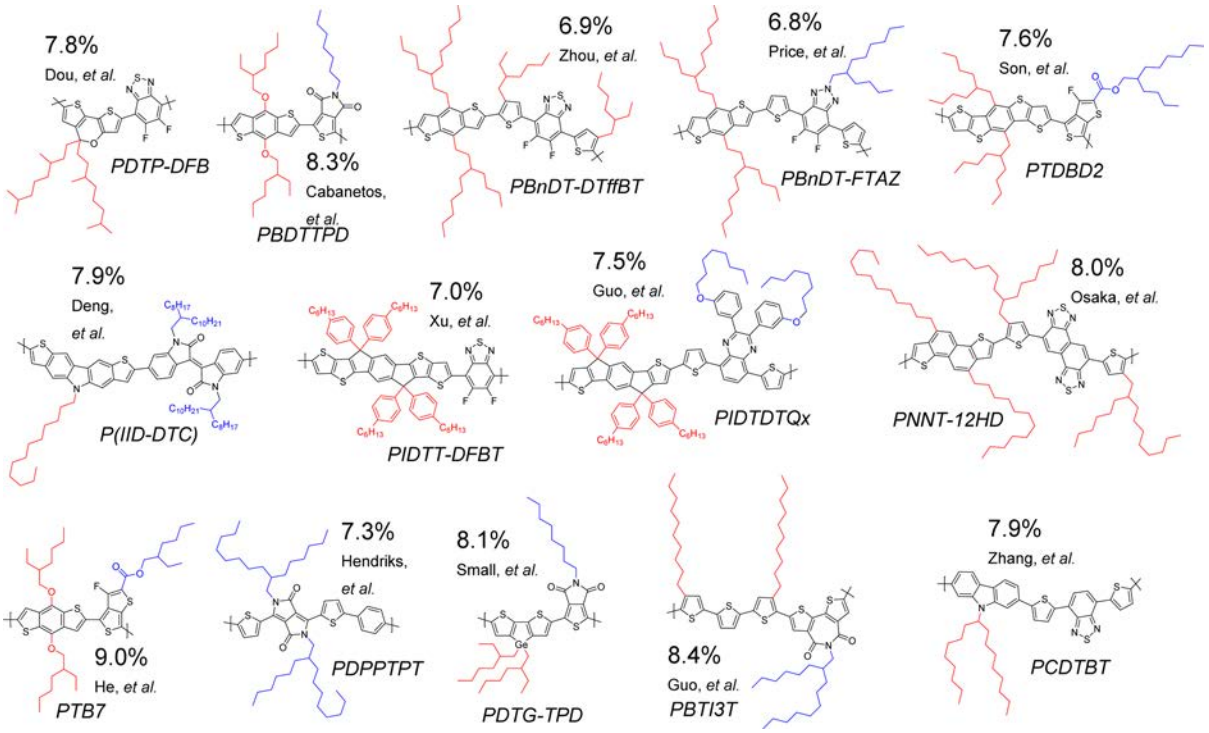

Figure 1. High-performing PV polymers and their power conversion efficiencies as reported in the literature, with red and blue substituents off the D and A moieties, respectively.[27−40]

role that this interfacial arrangement can play is apparent in the theoretical literature, where calculated electron transfer rates,[15] exciton binding energies,[16,17] interfacial energetics,[18−21] and charge separation probabilities[16,22] vary dramatically based on the molecular arrangement between electron-donating and electron-accepting molecules. Any one of these factors has the potential to greatly influence the performance of the OPV material system; however, probing the intermolecular arrangement is experimentally difficult, and thus its effects on device performance remain relatively untested.

The development of high-efficiency polymers and small molecules for PV applications has largely stemmed from the use of donor−acceptor (D−A) systems, whereby an electron-rich moiety ("donor") is covalently bound to an electron-deficient ("acceptor") moiety. In these D−A type systems the change in electron distribution between D and A moieties upon photoexcitation can vary substantially, depending on the strength of the D and A moieties; however, in most D−A polymers utilized in OPVs the LUMO tends to be more localized on the A moiety, whereas the HOMO tends to be more delocalized over the D and A moieties.[23] These D−A compounds, generally either polymers or oligomers, are the electron-donor materials in OPV devices, and usually a fullerene derivative is the electron-accepting material; thus, from here on "polymer" and "fullerene" will be used in reference to the electron-donating and electron-accepting materials, respectively, while donor and acceptor will be used in reference to the electron-rich and -deficient moieties of the electron-donating material. Among other reasons, these D−A compounds are advantageous owing to the precise control over the optical gap and energy levels of the frontier molecular orbitals that can be achieved through varying the strength of the D and A moieties.[6,24−26] Interestingly, a clear structural trend emerges in the alkyl substitution pattern for D−A compounds that show the highest performance in OPVs. That is, the donor moieties tend to have more bulky alkyl substituents, while the acceptor moieties have less bulky or no alkyl substituents. Herein, by combining literature trends among OPV materials with a systematic study of a set of specifically designed polymers, we explore the hypothesis that the highest performing polymers have a chemical structure that encourages the fullerenes to dock with the polymer in a specific location. Generally, this specific location appears to be with the A moiety of the polymer, though in a few select literature examples the specific location may be with the D moiety.

RESULTS AND DISCUSSION

Many of the highest performing polymers reported in the literature are highlighted in Figure 1.[27−40] The majority of these polymers have branched alkyl groups on the D moieties and either no or linear alkyl groups on the A moieties. This combination makes the A moieties more sterically accessible to the fullerene. For example, if a fullerene (essentially a ball of almost 1 nm diameter) is placed on top of each polymer backbone in Figure 1, the larger branched alkyl groups on the D moieties will sterically favor the fullerene to approach the A moieties. In **PTB7** and **PTDB2** there are branched alkyl groups on the A moieties, though these A moieties remain relatively accessible since the branch point is distanced from the conjugated backbone by a coplanar ester group.[41] The phenyl groups in **PIDTT−DFBT** and **PIDTDTQx** are out of plane, thereby providing significant steric hindrance over the center of the D moiety.[33] Some exceptions of where the A moiety is more sterically hindered are polymers containing amide groups, such as DPP, isoindigo (II), and BTI (see **PDPPTPT**, **P(IID-DTC)**, and **PBTI3T** in Figure 1, respectively). These exceptions may possibly be explained by a relatively strong interaction between amide groups and fullerenes that outweighs

dx.doi.org/10.1021/ja502985g | J. Am. Chem. Soc. 2014, 136, 9608−9618

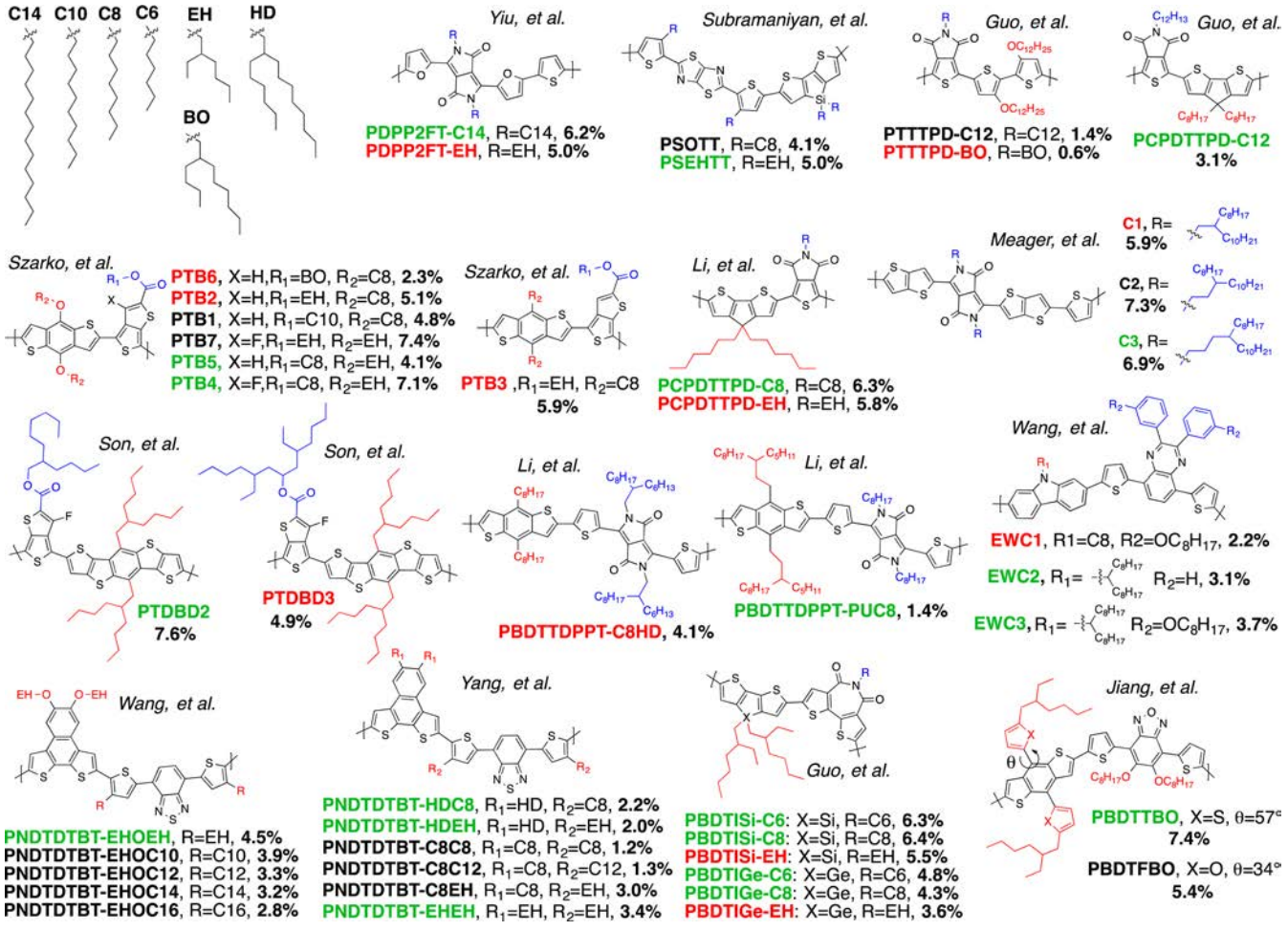

Figure 2. Donor polymers incorporated into polymer:fullerene bulk-heterojunction OPVs, wherein alkyl groups with varying bulkiness were utilized with the same conjugated backbone. Substituents are color coded in red or blue, depending on whether they are off the D or A moiety, respectively. The color of the polymer acronym indicates the relative predicted performance in a polymer family based on the hypothesis described above. Note that some polymers are renamed from their original work, the renaming strategy is PXXXYYY, where XXX is the donor moiety(s)' acronym(s) and YYY is the acceptor moiety's acronym.

the steric hindrance arising from the branched alkyl groups. This strong amide−fullerene interaction has previously been observed in solution state studies of fullerenes in or with amide-containing solvents.[42,43]

A possible alternative explanation for the prevalence of certain alkyl substitution patterns in high-performing PV polymers is that these derivatives are more synthetically accessible. However, an analysis of the PV performance of multiple polymer families, where the alkyl groups are varied while the polymer backbone is kept constant, emphasizes the importance of the polymer−fullerene arrangement. In the majority of these polymers, the highest performance is achieved for polymers where the A moiety is more sterically accessible and the D moiety more sterically hindered. These materials are shown in Figure 2 and their PV performance characteristics listed in Table 1. The polymers are compared only among similar derivatives reported in the same publication or reported by the same research group, with lines in Table 1 separating the polymer families. Within each polymer family, the polymer name is color-coded red, black, or green according to the performance trend that would be predicted on the basis of the hypothesis that the highest-performing material will result when the A moiety is more sterically accessible and/or the D moiety more sterically hindered. Red predicts a less sterically favorable polymer:fullerene arrangement with a more sterically accessible D moiety, black a more neutral arrangement with sterics not necessarily encouraging any particular arrangement, and green a favorable arrangement with the fullerene being encouraged to dock with the A moiety. The performance should thus increase from red to black to green, and as can be seen in Figure 2 and Table 1 the majority of polymers do follow the predicted trend.

All the polymers displayed in Figure 2 have been incorporated into bulk-heterojunction (BHJ) devices, with either $PC_{61}BM$ or $PC_{71}BM$ as the fullerene derivative. Considering these are all BHJ devices and the nanoscale morphology will significantly influence device performance, it is even more remarkable that the majority of the reported polymers follow the predicted trend. The two notable exceptions are the DPP containing **PBDTTDPPT** derivatives and some of the **PTB** derivatives. The reason these materials do not follow the predicted trend may be due to nanoscale morphology differences, differences in fullerene solubility in the mixed phase,[57] a sufficiently sterically accessible acceptor moiety in all derivatives, and/or favorable intermolecular interactions between the A moieties and the fullerene that lead to a preferred arrangement regardless of alkyl substitution pattern. The **PNDTDTBT−C8EH** derivative is listed as "maybe" in the table due to the bulky EH groups on the

dx.doi.org/10.1021/ja502985g | J. Am. Chem. Soc. 2014, 136, 9608−9618

Table 1. Performance of Organic Photovoltaic Cells for the Polymers Presented in Figure 2

Polymer	J_{SC} (mA/cm^2)	V_{OC} (V)	FF	PCE	Follows trend?	predicted
PDPP2FT-C14[44]	14.8	0.65	0.64	6.2	Yes	
PDPP2FT-EH[45]	11.2	0.74	0.60	5.0	Yes	
PSOTT[46]	10.2	0.62	0.65	4.1	Yes	
PSEHTT	12.6	0.65	0.61	5.0	Yes	
PTTTPD-C12[47]	7.36	0.41	0.48	1.44	Yes	
PTTTPD-BO	1.59	0.59	0.54	0.57	Yes	
PCPDTTPD-C12	8.12	0.76	0.50	3.06	Yes	
PTB6[48,49]	7.74	0.62	0.47	2.26	Yes	
PTB2	12.8	0.60	0.66	5.10	No	
PTB3	13.9	0.72	0.59	5.85	No	
PTB1	12.5	0.58	0.65	4.76	No	
PTB5	10.7	0.66	0.58	4.1	No	
PTB7[48]	14.5	0.74	0.69	7.4	Yes	
PTB4	15.5	0.70	0.65	7.1	Yes	
PCPDTTPD-C8[50]	14.1	0.75	0.61	6.31	Yes	
PCPDTTPD-EH	12.9	0.84	0.54	5.80	Yes	
C1[51]	16.6	0.59	0.60	5.9	Yes	
C2	18.6	0.61	0.64	7.3	Yes	
C3	18.7	0.60	0.62	6.9	Yes	
PTDBD2[28]	13.0	0.89	0.653	7.6	Yes	
PTDBD3	10.7	0.88	0.521	4.9	Yes	
PBDTTDPPT-C8HD[52]	9.4	0.71	0.61	4.1	No	
PBDTTDPPT-PUC8	5.2	0.62	0.43	1.4	No	
EWC1[53]	5.4	0.75	0.55	2.2	Yes	
EWC2	7.1	0.81	0.54	3.1	Yes	
EWC3	7.7	0.92	0.52	3.7	Yes	
PNDTDTBT-EHOEH[14]	10.5	0.70	0.61	4.5	Yes	
PNDTDTBT-EHOC10	9.36	0.68	0.63	3.9	Yes	
PNDTDTBT-EHOC12	7.85	0.68	0.58	3.3	Yes	
PNDTDTBT-EHOC14	7.35	0.73	0.59	3.2	Yes	
PNDTDTBT-EHOC16	6.64	0.67	0.63	2.8	Yes	
PNDTDTBT-HDC8[54]	7.98	0.59	0.461	2.17	Yes	
PNDTDTBT-HDEH	5.62	0.81	0.441	2.01	Yes	
PNDTDTBT-C8C8	6.97	0.41	0.421	1.20	Yes	
PNDTDTBT-C8C12	5.88	0.52	0.421	1.28	Yes	
PNDTDTBT-C8EH	10.93	0.59	0.464	3.00	Maybe	
PNDTDTBT-EHEH	10.67	0.69	0.459	3.36	Yes	

dx.doi.org/10.1021/ja502985g | J. Am. Chem. Soc. 2014, 136, 9608−9618

thiophenes pointing toward the central NDT donor moiety, and thereby providing some steric bulk around that moiety as well as the thiophenes. An alternative explanation regarding the role of a specific polymer:fullerene arrangement, which may not necessarily be fullerene docking with the A moiety, will be presented later in the manuscript and would encompass some of the aforementioned exceptions. Importantly, some of the polymers listed in Figure 2 and Table 1 that have a favorable alkyl substitution pattern still only have PCEs in the 3−4% range. These moderate PCEs highlight that an appropriate alkyl substitution pattern does not guarantee a high PCE, as several other properties, such as absorbance, blend film morphology, and charge-carrier mobilities, must also be optimized for a high-performing OPV material system.

In this work the family of **PBDTTPD** derivatives shown in Figure 3b are compared,[58−60] whereby the alkyl groups

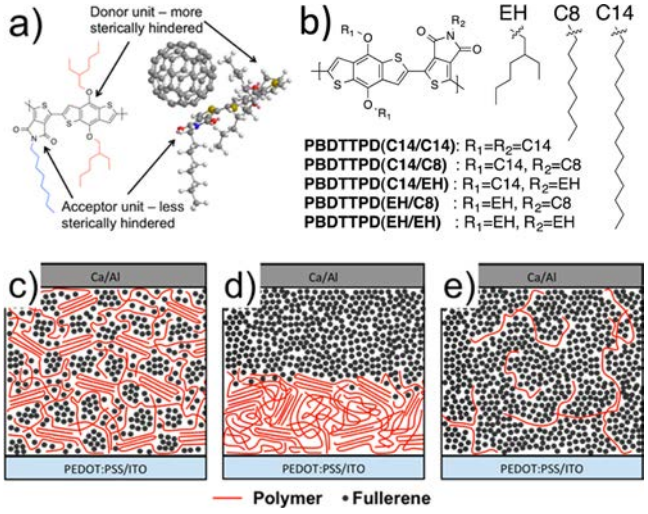

Figure 3. (a) Proposed model illustrating how branched alkyl groups on the donor unit direct the fullerene toward the acceptor unit in **PBDTTPD(EH/C8)**; (b) the **PBDTTPD** family of polymer derivatives designed to sterically favor different polymer:fullerene arrangements; and schematics of the (c) three-phase BHJ morphology,[57,62,63] (d) bilayer, and (e) low polymer content device architectures.

appended to the donor and acceptor moieties are either linear or branched. Varying the alkyl groups between linear C_8H_{17} (C8) or $C_{14}H_{29}$ (C14) and branched 2-ethylhexyl (EH) groups alters steric accessibility to the D and A units. As shown schematically in Figure 3a, the branched alkyl group is expected to provide steric hindrance and direct the fullerene to be closer to the linearly substituted unit. According to our hypothesis the highest performing derivative will have the branched EH group on BDT and the linear C8 group on TPD, referred to as **EH/C8**. The nomenclature used throughout this manuscript indicates the alkyl substituents on the BDT moiety followed by the substituent on the TPD moiety, i.e. **C14/C8** is the derivative where R_1 = C14 and R_2 = C8.

The materials were all synthesized in a similar manner to yield polymers with comparable impurities and end groups. Number-average molecular weights (M_n) are similar at 38, 38, and 36 kDa for the **C14/C14**, **C14/C8**, and **EH/C8** derivatives, respectively, and slightly lower at 21 and 19 kDa for the **C14/EH** and **EH/EH** derivatives, respectively. All polymers have similar PDIs of 1.7 to 2.0. The lower M_n of derivatives with EH on the TPD unit may result in some performance variations,[61] although the M_n alone is unlikely to explain the device results for the variety of device architectures presented herein. As shown in SI Figure S1, thin films of all the PBDTTPD derivatives show similar absorbance spectra with nearly identical optical gaps. These similarities in absorbance spectra suggest that varying the alkyl substitution pattern does not significantly affect electronic structure, molecular planarity, or conjugation length.

To experimentally test whether the OPV performance is in part determined by the molecular arrangement at the polymer:fullerene interface, the series of OPV device types presented in Figure 3c−e are examined. These include standard BHJ architectures with $PC_{61}BM$ as the electron-accepting material, bilayer OPV devices with C_{60} as the electron-accepting material, and low polymer concentration devices whereby 1−8 wt % of polymer is blended in a $PC_{61}BM$ matrix. The bilayer and low polymer concentration devices are included to reduce nanoscale morphology effects and minimize the influence of polymer−polymer interactions. In all device types the **EH/C8** derivative, where the branched substituent is on the BDT (donor) moiety and the linear substituent is on the TPD (acceptor) moiety, outperforms the other derivatives in terms of J_{SC} and overall PCE.

BHJ devices of the polymer:fullerene blends were all optimized for film thickness, polymer:fullerene ratio, and solvent additives for each individual polymer. All polymers showed similar optimized conditions, and therefore results are presented with identical fabrication conditions. As evident in Table 2 and the $J-V$ curves included in the SI, the **EH/C8** derivative outperforms the other materials in BHJ devices, with a 40−170% higher J_{SC} and a 1−38% higher FF vs the other derivatives. As a result, the PCE is 6.0% for the **EH/C8** derivative as compared to 3.8% for the next highest-performing

Table 2. Performance of Organic Photovoltaic Cells Based on BHJ and BL Architectures with Standard Deviations Indicated

material	architecture	J_{SC} (mA/cm^2)	V_{OC} (V)	FF	PCE (%)
C14/C14	BHJ	6.3 ± 0.1	0.94 ± 0.01	0.65 ± 0.07	3.8 ± 0.1
C14/C8	BHJ	6.9 ± 0.3	0.90 ± 0.02	0.53 ± 0.02	3.3 ± 0.2
C14/EH	BHJ	3.6 ± 0.2	0.97 ± 0.01	0.48 ± 0.03	1.7 ± 0.2
EH/C8	BHJ	9.6 ± 0.2	0.94 ± 0.01	0.66 ± 0.01	6.0 ± 0.3
EH/EH	BHJ	6.6 ± 0.4	0.96 ± 0.03	0.50 ± 0.03	3.2 ± 0.3
C14/C14	BL	1.3 ± 0.1	0.84 ± 0.02	0.63 ± 0.02	0.70 ± 0.03
C14/C8	BL	1.2 ± 0.1	0.80 ± 0.01	0.66 ± 0.01	0.63 ± 0.02
C14/EH	BL	1.5 ± 0.3	0.85 ± 0.01	0.58 ± 0.05	0.70 ± 0.08
EH/C8	BL	2.7 ± 0.3	0.87 ± 0.01	0.66 ± 0.01	1.5 ± 0.1
EH/EH	BL	2.1 ± 0.1	0.89 ± 0.03	0.58 ± 0.02	1.1 ± 0.1

dx.doi.org/10.1021/ja502985g | J. Am. Chem. Soc. 2014, 136, 9608−9618

derivative. The PCE of 6.0% for the **EH/C8** derivative is lower than can be achieved with $PC_{71}BM$ and comparable to the previous value reported with $PC_{61}BM$ and no solvent additives of 6.3%.[59] The higher performance for the **EH/C8** derivative is in agreement with the proposed model, although it is difficult to make any definitive conclusions from these trends, given the large number of variables contributing to the performance of a BHJ device. For example, the performance of a BHJ device depends strongly on the details of the nanoscale morphology, including the domain sizes and fullerene solubility in the mixed phase,[57,64,65] and these differences are nearly impossible to distinguish from other factors such as polymer:fullerene intermolecular arrangements. Bilayer device architectures, as shown in Figure 3d, were thus fabricated and tested to eliminate the effects of nanoscale morphology differences.

The results of bilayer (BL) OPV devices with a pure polymer layer and a thermally evaporated pure C_{60} layer are presented in Table 2 and Figure S3 in the SI. To minimize interfacial mixing between C_{60} and the polymers, the substrates were cooled down to ~0 °C during C_{60} deposition. Similar to the BHJ results, the **EH/C8** derivative outperforms the other derivatives with a PCE of 1.5% vs 1.1% for the next most efficient **EH/EH** derivative. The trends in these BL devices are relatively comparable to the trends in the BHJ devices with a few exceptions. The main exception is that the **C14/EH** derivative shows a PCE comparable to those of the linearly substituted **C14/C14** and **C14/C8** derivatives, whereby in the BHJ devices the J_{SC} and PCE of the **C14/EH**-based OPV device is only half that of the **C14/C14**-based device. This discrepancy between BHJ and BL device trends is most likely due to nanoscale morphology differences in the BHJ devices. The V_{OC} values for the BL devices are 0.07−0.10 V lower than the BHJ devices, which is likely the result of replacing $PC_{61}BM$ with the more electronegative C_{60}, as demonstrated previously for bilayer cells.[66]

To decrease the effects of polymer−polymer interactions present in the BHJ and bilayer devices, low polymer concentration devices with 1−8 wt % polymer in $PC_{61}BM$ were fabricated and characterized.[67] As shown schematically in Figure 3e, it is expected that predominantly isolated polymer strands are present as opposed to polymer aggregates. With the polymer backbones all being identical, and presumably minimal polymer−polymer interchain interactions, the differences in performance should be primarily related to how the polymers interact with the fullerene.

In these low polymer concentration devices the best performing polymer is again the **EH/C8** derivative. This derivative shows approximately twice the J_{SC} and PCE as the other derivatives in the 1, 2, 4, and 8% polymer devices as shown in Figure 4 and the $J-V$ curves in the SI. The relatively large standard deviations across multiple device sets may be attributed to variations in $PC_{61}BM$ batch and uncertainties associated with the low polymer concentrations (±15%). To probe whether or not differences in device performance can be attributed to a difference in the number of excitons reaching a polymer−fullerene interface, photoluminescence spectra of the blend films were measured. At a polymer concentration of 2% the fullerene emission is 34 ± 5% quenched for the **C14/EH**, **EH/C8**, and **EH/EH** blends and 26 ± 5% quenched in the **C14/C14** and **C14/C8** blends, as shown in SI Figure S6. This similar quenching behavior indicates performance differences are not likely due to an increased number of excitons reaching a polymer:fullerene interface. With similar exciton quenching

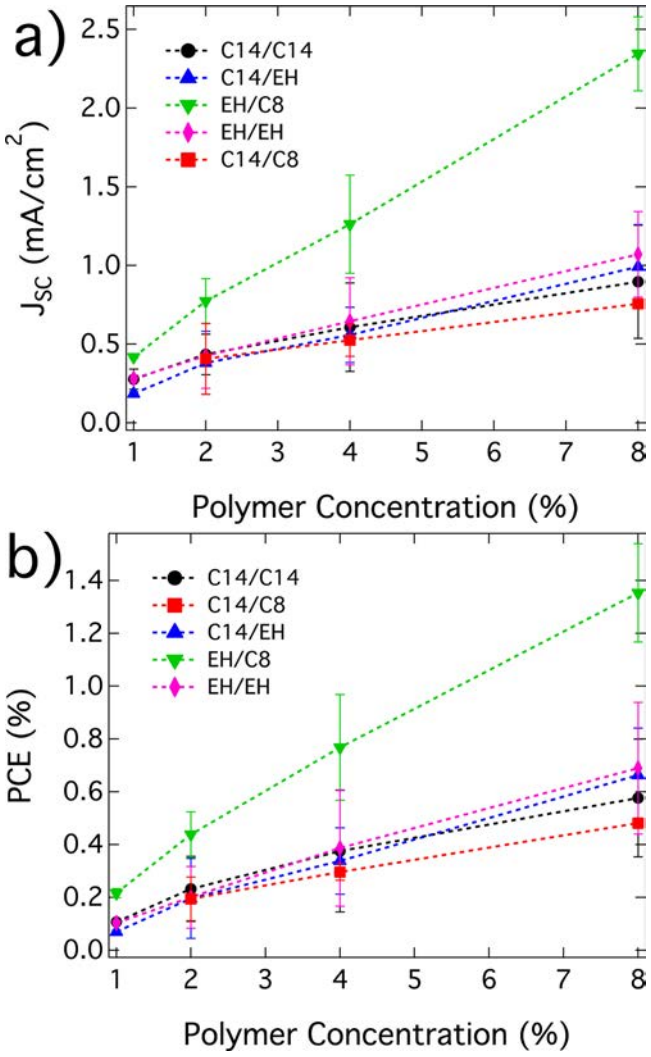

Figure 4. J_{SC} (a) and PCE (b) of polymer:$PC_{61}BM$ solar cells where the concentration of polymer was varied from 1 to 8% by weight relative to the total solids concentration. Error bars represent standard deviations of several device sets made with varying batches of $PC_{61}BM$.

behavior it is also likely that at this low polymer concentration there are not significant differences in the amount of polymer aggregation, which is expected to be minimal. At higher polymer concentrations of 4 and 8% some aggregation does occur as observed through transmission electron microscopy (TEM) and grazing incident wide-angle X-ray scattering (GIWAXS), see SI, although this does not change the trend in device performance.

To determine whether the performance differences are in part due to differences in nongeminate charge recombination dynamics, the charge-carrier lifetimes for nongeminate recombination were measured by transient photovoltage (TPV) as described by Shuttle, et al.[68] These TPV measurements were performed on PV devices with 2% polymer:98% $PC_{61}BM$, SI Figure S5, as in these devices polymer aggregation is minimized as compared to the 4 and 8% polymer devices. At one sun light intensity all polymers show a very similar lifetime of ~3 μs, with no correlation between short circuit current and charge-carrier lifetime. Furthermore, as a function of carrier density the charge-carrier lifetimes (τ) are almost identical for **EH/C8** and **EH/EH**. These similar bimolecular recombination lifetimes indicate that differences in PV performance cannot be

dx.doi.org/10.1021/ja502985g | J. Am. Chem. Soc. 2014, 136, 9608−9618

explained by differences in nongeminate recombination rates, thus leaving differences in geminate recombination as the most likely factor in differentiating the PV performance. With the same conjugated backbone, similar emission quenching behavior, similar bimolecular recombination dynamics, and predominantly polymer:fullerene interactions present, the most straightforward explanation for the differences in device performance is that the probability of charge separation or geminate recombination is dependent on the interfacial polymer:fullerene arrangement. Therefore, these results support the hypothesis that the highest performance of the **EH/C8** derivative originates from favorable docking of the fullerene with the A moiety of the polymer.

One method of directly probing the polymer:fullerene interfacial energetics is through the charge-transfer (CT) state absorbance, where the CT state is an intermolecular state formed between the polymer and fullerene.[69] This CT state can be probed with sensitive absorbance or EQE measurements, as shown in Figure 5. With interfacial energetics determined in part by intermolecular interactions, e.g. dipolar and quadrupolar,[19] the CT state absorbance is sensitive to the molecular arrangement at the polymer:fullerene interface. Figure 5 shows the CT region of the EQE spectra and fits to the CT band for the devices with polymer concentrations of 2 and 4%, where the data is fit with eq 1:[69,70]

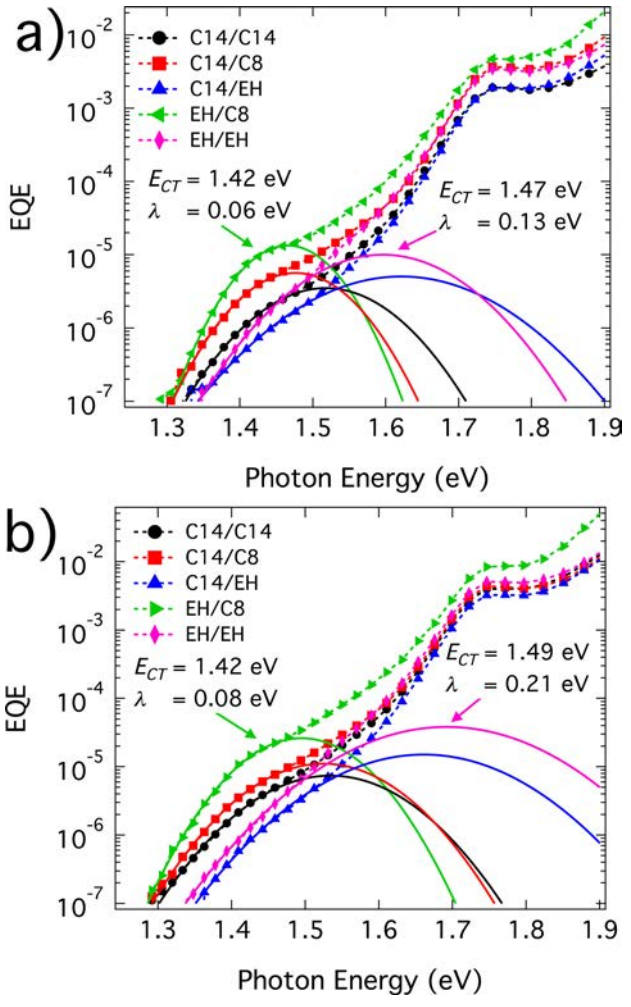

Figure 5. EQE spectra of the CT region, with fits to eq 1 indicated with solid lines, for polymer concentrations of (a) 2 and (b) 4%.

$$\mathrm{EQE} \propto \frac{f}{E\sqrt{4\pi\lambda kT}} \exp\left(\frac{-(E_{CT} + \lambda - E)^2}{4\lambda kT}\right) \quad (1)$$

Here, k is the Boltzmann constant, f is a term that accounts for the internal quantum efficiency, number of CT states, and electronic coupling, E_{CT} is an effective energy of the CT state, and λ is related to the width of the CT absorbance band. More specifically, λ contains a reorganization energy term (λ_0) that applies to a particular CT state environment and an energetic disorder term that reflects heterogeneities in CT state molecular arrangement and environment resulting from the restrictive, inhomogeneous solid-state film. λ_0 is the difference in energy between a vertically excited CT state with the same nuclear coordinates as the lowest-energy ground CT state and the energy minimum of the excited CT state after environmental (low frequency) and internal (high frequency) reorganization,[69,71,72] where in traditional liquid systems the environmental term is due to solvent reorganization. In the solid state, where inhomogeneous environments exist and nuclear positions are more constrained, the intermolecular arrangement and environment around each unique CT state can give rise to significant differences in absorbance and emission characteristics.[73,74] In a film consisting of many unique CT state environments these differences lead to greater optical peak widths and thereby increases in λ. Thus, in the polymer:$PC_{61}BM$ films analyzed here λ results from internal reorganization, environmental reorganization, and energetic disorder components. With the energy of a CT state depending on the molecular arrangement,[17,75] energetic disorder and λ will be reduced if a more specific molecular arrangement exists. From the fits of the data shown in Figure 5, we indeed find large differences in λ. For example, λ for the 4% **EH/C8**:$PC_{61}BM$ blend is 0.08 eV vs 0.21 eV for the 4% **EH/EH**:$PC_{61}BM$ blend

To confirm that energetic disorder contributes to λ, we investigate a system with a known low amount of disorder and a well-defined and specific polymer:fullerene arrangement, i.e. the PBTTT:$PC_{71}BM$ bimolecular crystal.[76] Analysis of the CT region of the EQE spectra for the PBTTT:$PC_{71}BM$ bimolecular crystal shows one of the narrowest CT absorbance bands of all BHJ systems, with λ of 0.12−0.13 eV (SI) compared to 0.2−0.4 eV for other BHJ systems.[69,77,78] This narrow CT absorbance band is indeed consistent with a more specific polymer−fullerene conformation.

As evident from Figure 5 and the SI, **EH/C8** in $PC_{61}BM$ shows the narrowest CT bands with λ of 0.06 and 0.08 eV for the 2 and 4% devices, respectively. This narrower CT band for the **EH/C8** derivative is in agreement with a more specific and consistent arrangement between polymer and fullerene, as a broader distribution of polymer:fullerene arrangements would increase the energetic distribution of CT states and increase λ. Displaying a slightly higher λ of 0.10 eV for the 2% polymer concentration device is the **C14/C14** derivative. When a branched chain is present on the TPD unit in **EH/EH**, λ is even higher at 0.13 eV for the 2% blend. A potential reason for this trend is that the EH group on TPD limits the otherwise energetically favorable TPD interaction with the fullerene, thus leading to a broader distribution of polymer:fullerene intermolecular arrangements. Another potential explanation for the decreased λ with the linear substituted TPD derivatives is that the fullerene is closer to the polymer backbone, as smaller center−center distances between molecules in a CT

dx.doi.org/10.1021/ja502985g | J. Am. Chem. Soc. 2014, 136, 9608−9618

complex will reduce the environmental reorganization term.[71] When the polymer concentration is increased to 8% the CT bands are broader for all polymers, with λ values of 0.2 to 0.3 eV. This broadening of the CT band most likely results from polymer aggregation occurring at these higher concentrations, where the aggregate regions of varying order would result in a wide spread of energy states. The narrower band at low concentration is another indicator that the majority of the polymers are more dispersed and minimally aggregated at low concentrations. The fact that all device types show the highest performance for the **EH/C8** derivative, regardless of the degree of polymer aggregation, is in agreement with the hypothesis that a specific polymer:fullerene arrangement leads to improved charge separation.

Solid-state nuclear magnetic resonance (NMR) spectroscopy complements the EQE measurements of the CT states by providing molecular-level insights on the interactions of the fullerene with the donor and acceptor moieties in the conjugated polymers. Specifically, solid-state two-dimensional (2D) $^{13}C\{^1H\}$ heteronuclear correlation (HETCOR) NMR measurements exploit through-space dipole−dipole couplings of locally proximate (<1 nm) ^{13}C and ^1H nuclei to correlate their isotropic chemical shifts. This provides direct information on intra- and key intermolecular interactions among the chemically distinct polymer and fullerene moieties shown in Figure 6a and b, which depicts the $PC_{61}BM$ functional groups (orange), the linear alkyl chains (blue), the branched EH alkyl groups (red), and the polymer backbone (brown). In particular, the 2D $^{13}C\{^1H\}$ HETCOR spectra of the neat **EH/C8** and **C14/EH** conjugated polymers and $PC_{61}BM$ (SI) yield well-resolved ^1H and ^{13}C signals that are confidently assigned to the specific polymer and $PC_{61}BM$ moieties, labeled in Figure 6a, as indicated above the respective 1D ^1H and ^{13}C MAS spectra in Figure 6c.

To gain insight into the polymer−fullerene intermolecular arrangement, 8 wt % polymer, 92% $PC_{61}BM$ blends were probed with 2D $^{13}C\{^1H\}$ HETCOR NMR. Although some aggregation is evident at 8 wt % polymer, these higher polymer concentrations are necessary to maximize the 2D $^{13}C\{^1H\}$ HETCOR signal arising from polymer−fullerene interactions. For the 8 wt % **EH/C8** in $PC_{61}BM$ blend, the 2D $^{13}C\{^1H\}$ HETCOR spectrum acquired at room temperature also yields well-resolved correlated signals, most of which reflect the same intramolecular contributions as for the neat components. Importantly, however, additional 2D intensity correlations are observed in Figure 6c that directly establish intermolecular interactions between the $PC_{61}BM$ and **EH/C8** polymer moieties. Specifically, ^{13}C signals associated with the C_{60} fullerene group at 140−148 ppm are strongly correlated with the ^1H signals at ∼1.2 ppm and ∼8.3 ppm (Figure 6c, red arrows) associated with the alkyl and aromatic ^1H moieties of the polymer, respectively. It is noteworthy that the only ^1H atoms on the polymer backbone are associated with carbon site 2 of the BDT unit, each of which is adjacent to a TPD moiety. Similar correlated intensities are observed in the 2D $^{13}C\{^1H\}$ spectrum (SI, Figure S9) of the 8 wt % **C14/EH** in $PC_{61}BM$ blend. These 2D intensity correlations unambiguously establish the close (<1 nm) proximities of the C_{60} moieties of the $PC_{61}BM$ molecules to the polymer backbone for both of the **EH/C8** and **C14/EH** heterojunction blends, as required for efficient charge transfer.

The 2D NMR results furthermore suggest that the type and placement of the alkyl groups influence the local configurations

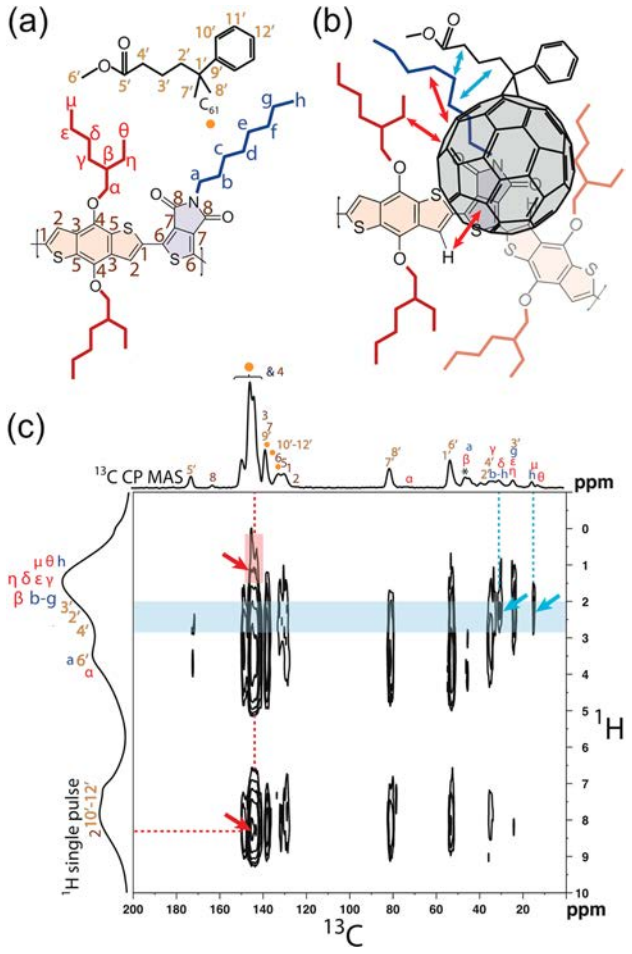

Figure 6. Molecular structures of (a) **EH/C8** and $PC_{61}BM$, with their respective moieties labeled and (b) schematic showing red and blue arrows that indicate intermolecular interactions between the conjugated polymer and $PC_{61}BM$ moieties that are consistent with the 2D NMR intensity correlations. (c) Solid-state 2D $^{13}C\{^1H\}$ dipolar-mediated heteronuclear correlation (HETCOR) NMR spectrum acquired at room temperature for an 8 wt % **EH/C8** in $PC_{61}BM$ blend under MAS conditions of 12.5 kHz, with an 8 ms CP contact time. One dimensional $^{13}C\{^1H\}$ CPMAS and single-pulse ^1H MAS spectra are shown along the top horizontal axis and the left vertical axis, respectively.

of the $PC_{61}BM$ moieties near the polymer backbone. In particular, the ^{13}C signals at 31 and 14 ppm that are associated with carbon atoms *b*−*f* and *h*, respectively, of the linear C8 alkyl chains on the TPD acceptor moiety are strongly correlated (Figure 6c, blue arrows) with the ^1H signals at 2−3 ppm from moieties 2′−4′ of the $PC_{61}BM$ functional group (Figure 6c, blue band). While the ^{13}C signal at 31 ppm contains overlapping signals from carbon atoms *b*−*f* of the linear C8 alkyl chain and δ of the branched EH alkyl groups, most of this signal intensity appears to arise from the ^{13}C atoms of the C8 chains (5/TPD moiety), as opposed to those of the EH groups (2/BDT moiety). This is evident from comparison with the 2D $^{13}C\{^1H\}$ HETCOR spectrum (SI) for the 8 wt % **C14/EH** in $PC_{61}BM$ blend, in which significantly greater intensity is observed in the correlated signals at 31 ppm in the ^{13}C dimension and at 2−3 ppm in the ^1H dimension. This is consistent with the greater population of interior ^{13}C atoms of the linear C14 chains (22/BDT moiety) relative to the δ-type carbon atoms in the branched EH alkyl groups (1/TPD

dx.doi.org/10.1021/ja502985g | J. Am. Chem. Soc. 2014, 136, 9608−9618

moiety) and also compared to the **EH/C8** blend. Moreover, the association of the ^{13}C signals at 31 ppm with linear alkyl moieties is also evidenced by the different relative intensities of the weaker correlated signals at 14 ppm (^{13}C) and 2−3 ppm (^{1}H), which are consistent with the comparable populations of moieties μ, h, and n in the two blends (SI Figure S13). These results collectively indicate that, in both blend materials, the $PC_{61}BM$ functional groups interact to greater extents with the linear C8 or C14 alkyl chains of the polymers, compared to the branched EH alkyl groups. As the polymer alkyl chains are covalently bonded to either the TPD or BDT moieties of the polymer backbone, the strong intensity correlations between the linear alkyl chains and $PC_{61}BM$ functional groups suggest that $PC_{61}BM$ species are in closer proximity to moieties of the polymer backbone that have linear alkyl chains, as opposed to those with branched EH groups. The 2D NMR analyses thus establish close (<1 nm) proximities of the $PC_{61}BM$ molecules with the polymer backbone and the linear alkyl chains, which provide evidence of preferential interactions of the $PC_{61}BM$ species and the TPD acceptor moieties in the **EH/C8** blend, as depicted in the schematic diagram of Figure 6b.

Overall, the collective data presented here demonstrate that PBDTTPD derivatives perform better in OPV devices when the fullerene is closer to the electron-accepting TPD moiety. One explanation of why this polymer:fullerene arrangement is beneficial is that the resulting intermolecular interactions create a favorable energy landscape, either the result of a partial charge transfer, dipole−induced dipole, or quadrupolar interactions. Theoretically, it has been shown that the interface dipole, as well as the energetics of molecules near the interface, can vary by hundreds of meV depending on the donor:fullerene arrangement.[4,18,19,21,79,80] Variations in energy levels, combined with how charges are stabilized or destabilized by induced dipoles and quadrupolar interactions, can lead to near zero electron−hole binding energies with certain interfacial molecular arrangements.[16,18,19] These energetic shifts arising from intermolecular interactions may be a key factor in providing an energetic driving force for charges to move away from the polymer:fullerene interface, or out of the mixed phase in a 3-phase BHJ system.[57,62,63] Another potential explanation is that the wave function overlap leads to high rates of charge transfer and low rates of charge recombination when the fullerene is in closer proximity to the acceptor unit. Both lower rates of charge recombination and interfacial energetic offsets have been shown with Monte Carlo simulations to increase the probability of charge separation,[81,82] and it is indeed possible that either or both of these factors may explain the performance trend observed for the PBDTTPD derivatives. Yet another potential explanation is that, when the fullerene docks with a specific part of the polymer, either donor or acceptor moiety, the energetic disorder in both the polymer and fullerene sites are reduced. Decreased energetic disorder should increase the probability of charge separation, as the local charge-carrier mobilities will remain high and there will not be energetic barriers between lower- and higher-energy sites. In this explanation of a specific intermolecular arrangement leading to decreased energetic disorder, which results in an improved probability for charge separation, it may not be as critical as to what the arrangement is as long as it is consistent. These potential explanations highlight the need for further theoretical and experimental studies to bring about a better molecular level understanding of the variables influencing charge separation and OPV performance.

CONCLUSION

It remains difficult to fully design OPV materials, in part because some of the molecular factors influencing charge separation are not yet known. The literature and work presented here suggests that a preferred intermolecular arrangement exists in high-performing OPV polymer:fullerene systems, where the fullerene is generally docked with the electron-accepting moiety of the polymer. Identification of this trend helps to establish why certain alkyl substitution patterns have led to successful polymers and will aid in the more directed design of future materials. For example, new materials should likely be designed with the electron-accepting moiety of the polymer being more sterically accessible and the electron-donating moiety more sterically hindered, and/or acceptor moieties that interact favorably with the fullerene should be identified and utilized. Observation of this trend paves the way for further theoretical and experimental studies, including determination of the intermolecular energy landscape, how this energetic landscape effects charge separation, what intermolecular interactions lead to a favorable energy landscape, and how factors such as interfacial energetic disorder influence charge separation. Determination of these factors will prove critical in guiding the design of future high-efficiency OPV material systems.

ASSOCIATED CONTENT

Supporting Information

Experimental details and procedures, synthetic details, current−voltage and PV performance characteristics, EQE data, TEM images, GIWAXS plots, 2D $^{13}C\{^{1}H\}$ HETCOR NMR data, photoluminescence data. This material is available free of charge via the Internet at http://pubs.acs.org.

AUTHOR INFORMATION

Corresponding Authors

aram.amassian@kaust.edu.sa (A.A.)
pierre.beaujuge@kaust.edu.sa (P.M.B.)
mmcgehee@stanford.edu (M.D.M.)

Notes

The authors declare no competing financial interest.

ACKNOWLEDGMENTS

This publication was supported by the Center for Advanced Molecular Photovoltaics (Award No KUS-C1-015-21) and was made possible by King Abdullah University of Science and Technology (KAUST). K.R.G. and A.A. acknowledge SABIC for a postdoctoral fellowship. G.O.N.N., K.R.G., M.D.M., and A.A. acknowledge the Office of Competitive Research Funds for a GRP-CF award. T.H. gratefully acknowledges a "DAAD Doktorantenstipendium" and the SFB 953 "Synthetic Carbon Allotropes". Use of the Stanford Synchrotron Radiation Lightsource, SLAC National Accelerator Laboratory, is supported by the U.S. Department of Energy, Office of Science, Office of Basic Energy Sciences under Contract No. DE-AC02-76SF00515. The NMR experiments were conducted in the Central Facilities of the UCSB Materials Research Laboratory supported by the MRSEC program of the U.S. NSF under Award No. DMR-1121053. The work at UCSB was supported by the USARO through the Institute for Collaborative Biotechnologies under Contract No. W911NF-09-D-0001. The authors also thank Dr. Chad Risko and Prof. Jean-Luc Brédas for helpful discussions.

REFERENCES

(1) Dou, L.; You, J.; Hong, Z.; Xu, Z.; Li, G.; Street, R. A.; Yang, Y. *Adv. Mater.* **2013**, *25*, 6642.
(2) Darling, S. B.; You, F. *RSC Adv.* **2013**, *3*, 17633.
(3) Angmo, D.; Gevorgyan, S. A.; Larsen-Olsen, T. T.; Søndergaard, R. R.; Hösel, M.; Jørgensen, M.; Gupta, R.; Kulkarni, G. U.; Krebs, F. C. *Org. Electron.* **2013**, *14*, 984.
(4) Beljonne, D.; Cornil, J.; Muccioli, L.; Zannoni, C.; Brédas, J.-L.; Castet, F. *Chem. Mater.* **2011**, *23*, 591.
(5) Jørgensen, M.; Carlé, J. E.; Søndergaard, R. R.; Lauritzen, M.; Dagnæs-Hansen, N. a.; Byskov, S. L.; Andersen, T. R.; Larsen-Olsen, T. T.; Böttiger, A. P. L.; Andreasen, B.; Fu, L.; Zuo, L.; Liu, Y.; Bundgaard, E.; Zhan, X.; Chen, H.; Krebs, F. C. *Sol. Energy Mater. Sol. Cells* **2013**, *119*, 84.
(6) Zhou, H.; Yang, L.; You, W. *Macromolecules* **2012**, *45*, 607.
(7) Beaujuge, P. M.; Fréchet, J. M. J. *J. Am. Chem. Soc.* **2011**, *133*, 20009.
(8) Mishra, A.; Bäuerle, P. *Angew. Chem., Int. Ed.* **2012**, *51*, 2020.
(9) Guo, X.; Zhou, N.; Lou, S. J.; Hennek, J. W.; Ponce Ortiz, R.; Butler, M. R.; Boudreault, P.-L. T.; Strzalka, J.; Morin, P.-O.; Leclerc, M.; López Navarrete, J. T.; Ratner, M. A.; Chen, L. X.; Chang, R. P. H.; Facchetti, A.; Marks, T. J. *J. Am. Chem. Soc.* **2012**, *134*, 18427.
(10) Li, Y.; Zou, J.; Yip, H.; Li, C.; Zhang, Y.; Chueh, C.; Intemann, J.; Xu, Y.; Liang, P.; Chen, Y.; Jen, A. K.-Y. *Macromolecules* **2013**, *46*, 5497.
(11) Carsten, B.; Szarko, J. M.; Son, H. J.; Wang, W.; Lu, L.; He, F.; Rolczynski, B. S.; Lou, S. J.; Chen, L. X.; Yu, L. *J. Am. Chem. Soc.* **2011**, *133*, 20468.
(12) Carsten, B.; Szarko, J. M.; Lu, L.; Son, H. J.; He, F.; Botros, Y. Y.; Chen, L. X.; Yu, L. *Macromolecules* **2012**, *45*, 6390.
(13) Hong, Y.-R.; Wong, H.-K.; Moh, L. C. H.; Tan, H.-S.; Chen, Z.-K. *Chem. Commun.* **2011**, *47*, 4920.
(14) Wang, B.; Zhang, J.; Tam, H. L.; Wu, B.; Zhang, W.; Chan, M. S.; Pan, F.; Yu, G.; Zhu, F.; Wong, M. S. *Polym. Chem.* **2013**, *5*, 836.
(15) Yi, Y.; Coropceanu, V.; Brédas, J.-L. *J. Am. Chem. Soc.* **2009**, *131*, 15777.
(16) Verlaak, S.; Beljonne, D.; Cheyns, D.; Rolin, C.; Linares, M.; Castet, F.; Cornil, J.; Heremans, P. *Adv. Funct. Mater.* **2009**, *19*, 3809.
(17) Yost, S. R.; Wang, L.-P.; Van Voorhis, T. *J. Phys. Chem. C* **2011**, *115*, 14431.
(18) Linares, M.; Beljonne, D.; Cornil, J.; Lancaster, K.; Brédas, J.-L.; Verlaak, S.; Mityashin, A.; Heremans, P.; Fuchs, A.; Lennartz, C.; Idé, J.; Méreau, R.; Aurel, P.; Ducasse, L.; Castet, F. *J. Phys. Chem. C* **2010**, *114*, 3215.
(19) Idé, J.; Mothy, S.; Savoyant, A.; Fritsch, A.; Aurel, P.; Méreau, R.; Ducasse, L.; Cornil, J.; Beljonne, D.; Castet, F. *Int. J. Quantum Chem.* **2013**, *113*, 580.
(20) Chen, W.; Qi, D.-C.; Huang, H.; Gao, X.; Wee, A. T. S. *Adv. Funct. Mater.* **2011**, *21*, 410.
(21) Heimel, G.; Salzmann, I.; Duhm, S.; Koch, N. *Chem. Mater.* **2011**, *23*, 359.
(22) Rand, B. P.; Cheyns, D.; Vasseur, K.; Giebink, N. C.; Mothy, S.; Yi, Y.; Coropceanu, V.; Beljonne, D.; Cornil, J.; Brédas, J.-L.; Genoe, J. *Adv. Funct. Mater.* **2012**, *22*, 2987.
(23) Risko, C.; McGehee, M. D.; Brédas, J.-L. *Chem. Sci.* **2011**, *2*, 1200.
(24) Zhou, Q.; Hou, Q.; Zheng, L.; Deng, X.; Yu, G.; Cao, Y. *Appl. Phys. Lett.* **2004**, *84*, 1653.
(25) Beaujuge, P. M.; Amb, C. M.; Reynolds, J. R. *Acc. Chem. Res.* **2010**, *43*, 1396.
(26) Ellinger, S.; Graham, K. R.; Shi, P.; Farley, R. T.; Steckler, T. T.; Brookins, R. N.; Taranekar, P.; Mei, J.; Padilha, L. A.; Ensley, T. R.; Hu, H.; Webster, S.; Hagan, D. J.; Van Stryland, E. W.; Schanze, K. S.; Reynolds, J. R. *Chem. Mater.* **2011**, *23*, 3805.
(27) He, Z.; Zhong, C.; Su, S.; Xu, M.; Wu, H.; Cao, Y. *Nat. Photonics* **2012**, *6*, 593.
(28) Son, H. J.; Lu, L.; Chen, W.; Xu, T.; Zheng, T.; Carsten, B.; Strzalka, J.; Darling, S. B.; Chen, L. X.; Yu, L. *Adv. Mater.* **2013**, *25*, 838.
(29) Zhou, H.; Yang, L.; Stuart, A. C.; Price, S. C.; Liu, S.; You, W. *Angew. Chem., Int. Ed.* **2011**, *50*, 2995.
(30) Price, S. C.; Stuart, A. C.; Yang, L.; Zhou, H.; You, W. *J. Am. Chem. Soc.* **2011**, *133*, 4625.
(31) Zhang, Y.; Zhou, H.; Seifter, J.; Ying, L.; Mikhailovsky, A.; Heeger, A. J.; Bazan, G. C.; Nguyen, T.-Q. *Adv. Mater.* **2013**, *25*, 7038.
(32) Osaka, I.; Kakara, T.; Takemura, N.; Koganezawa, T.; Takimiya, K. *J. Am. Chem. Soc.* **2013**, *135*, 8834.
(33) Xu, Y.-X.; Chueh, C.-C.; Yip, H.-L.; Ding, F.-Z.; Li, Y.-X.; Li, C.-Z.; Li, X.; Chen, W.-C.; Jen, A. K.-Y. *Adv. Mater.* **2012**, *24*, 6356.
(34) Guo, X.; Zhang, M.; Tan, J.; Zhang, S.; Huo, L.; Hu, W.; Li, Y.; Hou, J. *Adv. Mater.* **2012**, *24*, 6536.
(35) Dou, L.; Chen, C.-C.; Yoshimura, K.; Ohya, K.; Chang, W.-H.; Gao, J.; Liu, Y.; Richard, E.; Yang, Y. *Macromolecules* **2013**, *46*, 3384.
(36) Hendriks, K. H.; Heintges, G. H. L.; Gevaerts, V. S.; Wienk, M. M.; Janssen, R. A. J. *Angew. Chem., Int. Ed.* **2013**, *52*, 8341.
(37) Cabanetos, C.; El Labban, A.; Bartelt, J. A.; Douglas, J. D.; Mateker, W. R.; Fréchet, J. M. J.; McGehee, M. D.; Beaujuge, P. M. *J. Am. Chem. Soc.* **2013**, *135*, 4656.
(38) Small, C. E.; Chen, S.; Subbiah, J.; Amb, C. M.; Tsang, S.; Lai, T.; Reynolds, J. R.; So, F. *Nat. Photonics* **2011**, *6*, 115.
(39) Guo, X.; Zhou, N.; Lou, S. J.; Smith, J.; Tice, D. B.; Hennek, J. W.; Ortiz, R. P.; Navarrete, J. T. L.; Li, S.; Strzalka, J.; Chen, L. X.; Chang, R. P. H.; Facchetti, A.; Marks, T. J. *Nat. Photonics* **2013**, *7*, 825.
(40) Deng, Y.; Liu, J.; Wang, J.; Liu, L.; Li, W.; Tian, H.; Zhang, X.; Xie, Z.; Geng, Y.; Wang, F. *Adv. Mater.* **2014**, *26*, 471.
(41) Niklas, J.; Mardis, K. L.; Banks, B. P.; Grooms, G. M.; Sperlich, A.; Beaupre, S.; Dyakonov, V.; Beaupré, S.; Leclerc, M.; Xu, T.; Yu, L.; Poluektov, O. G. *Phys. Chem. Chem. Phys.* **2013**, *15*, 9562.
(42) Alfè, M.; Apicella, B.; Barbella, R.; Bruno, A.; Ciajolo, A. *Chem. Phys. Lett.* **2005**, *405*, 193.
(43) Aksenov, V. L.; Tropin, T. V.; Kyzyma, O. A.; Avdeev, M. V.; Korobov, M. V.; Rosta, L. *Phys. Solid State* **2010**, *52*, 1059.
(44) Yiu, A. T.; Beaujuge, P. M.; Lee, O. P.; Woo, C. H.; Toney, M. F.; Fréchet, J. M. J. *J. Am. Chem. Soc.* **2012**, *134*, 2180.
(45) Woo, C. H.; Beaujuge, P. M.; Holcombe, T. W.; Lee, O. P.; Fréchet, J. M. J. *J. Am. Chem. Soc.* **2010**, *132*, 15547.
(46) Subramaniyan, S.; Xin, H.; Kim, F. S.; Shoaee, S.; Durrant, J. R.; Jenekhe, S. A. *Adv. Energy Mater.* **2011**, *1*, 854.
(47) Guo, X.; Xin, H.; Kim, F. S.; Liyanage, A. D. T.; Jenekhe, S. A.; Watson, M. D. *Macromolecules* **2011**, *44*, 269.
(48) Szarko, J. M.; Guo, J.; Liang, Y.; Lee, B.; Rolczynski, B. S.; Strzalka, J.; Xu, T.; Loser, S.; Marks, T. J.; Yu, L.; Chen, L. X. *Adv. Mater.* **2010**, *22*, 5468.
(49) Liang, Y.; Feng, D.; Wu, Y.; Tsai, S.-T.; Li, G.; Ray, C.; Yu, L. *J. Am. Chem. Soc.* **2009**, *131*, 7792.
(50) Li, Z.; Tsang, S.-W.; Du, X.; Scoles, L.; Robertson, G.; Zhang, Y.; Toll, F.; Tao, Y.; Lu, J.; Ding, J. *Adv. Funct. Mater.* **2011**, *21*, 3331.
(51) Meager, I.; Ashraf, R. S.; Mollinger, S.; Schroeder, B. C.; Bronstein, H.; Beatrup, D.; Vezie, M. S.; Kirchartz, T.; Salleo, A.; Nelson, J.; McCulloch, I. *J. Am. Chem. Soc.* **2013**, *135*, 11537.
(52) Li, Z.; Zhang, Y.; Tsang, S.-W.; Du, X.; Zhou, J.; Tao, Y.; Ding, J. *J. Phys. Chem. C* **2011**, *115*, 18002.
(53) Wang, E.; Hou, L.; Wang, Z.; Ma, Z.; Hellstr, S.; Zhuang, W.; Zhang, F.; Ingan, O.; Andersson, M. R. *Macromolecules* **2011**, *44*, 2067.
(54) Yang, L.; Zhou, H.; You, W. *J. Phys. Chem. C* **2010**, *114*, 16793.
(55) Guo, X.; Zhou, N.; Lou, S. J.; Hennek, J. W.; Ponce Ortiz, R.; Butler, M. R.; Boudreault, P.-L. T.; Strzalka, J.; Morin, P.-O.; Leclerc, M.; López Navarrete, J. T.; Ratner, M. A.; Chen, L. X.; Chang, R. P. H.; Facchetti, A.; Marks, T. J. *J. Am. Chem. Soc.* **2012**, *134*, 18427.
(56) Jiang, J.-M. J.; Lin, H.-K. H.; Lin, Y.-C. Y.; Chen, H. H.-C.; Lan, S.-C.; Chang, C.-K.; Wei, K.-H. *Macromolecules* **2014**, *47*, 70.
(57) Bartelt, J. A.; Beiley, Z. M.; Hoke, E. T.; Mateker, W. R.; Douglas, J. D.; Collins, B. A.; Tumbleston, J. R.; Graham, K. R.; Amassian, A.; Ade, H.; Fréchet, J. M. J.; Toney, M. F.; McGehee, M. D. *Adv. Energy Mater.* **2013**, *3*, 364.
(58) Zou, Y.; Najari, A.; Berrouard, P.; Beaupré, S.; Aïch, B. R.; Tao, Y.; Leclerc, M. *J. Am. Chem. Soc.* **2010**, *132*, 5330.

(59) Piliego, C.; Holcombe, T. W.; Douglas, J. D.; Woo, C. H.; Beaujuge, P. M.; Fréchet, J. M. J. *J. Am. Chem. Soc.* **2010**, *132*, 7595.
(60) Zhang, Y.; Hau, S. K.; Yip, H.-L.; Sun, Y.; Acton, O.; Jen, A. K.-Y. *Chem. Mater.* **2010**, *22*, 2696.
(61) Bartelt, J. A.; Douglas, J. D.; Mateker, W. R.; Labban, A. E.; Tassone, C. J.; Toney, M. F.; Fréchet, J. M. J.; Beaujuge, P. M.; McGehee, M. D. *Adv. Energy Mater.* **2014**, DOI: 10.1002/aenm.201301733.
(62) Shoaee, S.; Subramaniyan, S.; Xin, H.; Keiderling, C.; Tuladhar, P. S.; Jamieson, F.; Jenekhe, S. A.; Durrant, J. R. *Adv. Funct. Mater.* **2013**, *23*, 3286.
(63) Westacott, P.; Tumbleston, J. R.; Shoaee, S.; Fearn, S.; aaBannock, J. H.; Gilchrist, J. B.; Heutz, S.; deMello, J.; Heeney, M.; Ade, H.; Durrant, J.; McPhail, D. S.; Stingelin, N. *Energy Environ. Sci.* **2013**, *6*, 2756.
(64) Amb, C. M.; Chen, S.; Graham, K. R.; Subbiah, J.; Small, C. E.; So, F.; Reynolds, J. R. *J. Am. Chem. Soc.* **2011**, *133*, 10062.
(65) Treat, N. D.; Varotto, A.; Takacs, C. J.; Batara, N.; Al-Hashimi, M.; Heeney, M. J.; Heeger, A. J.; Wudl, F.; Hawker, C. J.; Chabinyc, M. L. *J. Am. Chem. Soc.* **2012**, *134*, 15869.
(66) Chu, C.-W.; Shrotriya, V.; Li, G.; Yang, Y. *Appl. Phys. Lett.* **2006**, *88*, 153504.
(67) Yang, B.; Guo, F.; Yuan, Y.; Xiao, Z.; Lu, Y.; Dong, Q.; Huang, J. *Adv. Mater.* **2013**, *25*, 572.
(68) Shuttle, C. G.; O'Regan, B.; Ballantyne, A. M.; Nelson, J.; Bradley, D. D. C.; de Mello, J.; Durrant, J. R. *Appl. Phys. Lett.* **2008**, *92*, 093311.
(69) Vandewal, K.; Tvingstedt, K.; Gadisa, A.; Inganäs, O.; Manca, J. V. *Phys. Rev. B* **2010**, *81*, 125204.
(70) Graham, K. R.; Erwin, P.; Nordlund, D.; Vandewal, K.; Li, R.; Ngongang Ndjawa, G. O.; Hoke, E. T.; Salleo, A.; Thompson, M. E.; McGehee, M. D.; Amassian, A. *Adv. Mater.* **2013**, *25*, 6076.
(71) Marcus, R. A. *J. Phys. Chem.* **1990**, *94*, 4963.
(72) Brunschwig, B. S.; Ehrenson, S.; Sutin, N. *J. Phys. Chem.* **1987**, *91*, 4714.
(73) Hou, Y.; Bardo, A. M.; Martinez, C.; Higgins, D. A. *J. Phys. Chem. B* **2000**, *104*, 212.
(74) Rhodes, T. A.; Farid, S.; Goodman, J. L.; Gould, I. R.; Young, R. H. *J. Am. Chem. Soc.* **1999**, *121*, 5340.
(75) Ojala, A.; Petersen, A.; Fuchs, A.; Lovrincic, R.; Pölking, C.; Trollmann, J.; Hwang, J.; Lennartz, C.; Reichelt, H.; Höffken, H. W.; Pucci, A.; Erk, P.; Kirchartz, T.; Würthner, F. *Adv. Funct. Mater.* **2012**, *22*, 86.
(76) Miller, N. C.; Cho, E.; Junk, M. J. N.; Gysel, R.; Risko, C.; Kim, D.; Sweetnam, S.; Miller, C. E.; Richter, L. J.; Kline, R. J.; Heeney, M.; McCulloch, I.; Amassian, A.; Acevedo-Feliz, D.; Knox, C.; Hansen, M. R.; Dudenko, D.; Chmelka, B. F.; Toney, M. F.; Brédas, J.-L.; McGehee, M. D. *Adv. Mater.* **2012**, *24*, 6071.
(77) Ko, S.; Hoke, E. T.; Pandey, L.; Hong, S.; Mondal, R.; Risko, C.; Yi, Y.; Noriega, R.; McGehee, M. D.; Brédas, J.-L.; Salleo, A.; Bao, Z. *J. Am. Chem. Soc.* **2012**, *134*, 5222.
(78) Piersimoni, F.; Chambon, S.; Vandewal, K.; Mens, R.; Boonen, T.; Gadisa, A.; Izquierdo, M.; Filippone, S.; Ruttens, B.; D'Haen, J.; Martin, N.; Lutsen, L.; Vanderzande, D.; Adriaensens, P.; Manca, J. V. *J. Phys. Chem. C* **2011**, *115*, 10873.
(79) Mothy, S.; Guillaume, M.; Idé, J.; Castet, F.; Ducasse, L.; Cornil, J.; Beljonne, D. *J. Phys. Chem. Lett.* **2012**, *3*, 2374.
(80) D'Avino, G.; Mothy, S.; Muccioli, L.; Zannoni, C.; Wang, L.; Cornil, J.; Beljonne, D.; Castet, F. *J. Phys. Chem. C* **2013**, *117*, 12981.
(81) Burke, T. M.; McGehee, M. D. *Adv. Mater.* **2014**, *26*, 1923.
(82) Groves, C. *Energy Environ. Sci.* **2013**, *6*, 1546.